POLITECNICO DI TORINO
Repository ISTITUZIONALE

Impulsive current test method for characterizing discharge behavior in conductive textiles

Original
Impulsive current test method for characterizing discharge behavior in conductive textiles / Rossi, A., Rimondotto, N., Franchini, F., Ferraris, L., Lavagna, L., Pavese, M.. - In: MATERIALS SCIENCE AND ENGINEERING B-SOLID STATE MATERIALS FOR ADVANCED TECHNOLOGY. - ISSN 0921-5107. - ELETTRONICO. - 333:(2026), pp. 1-12. [10.1016/j.mseb.2026.119787]

Availability:
This version is available at: 11583/3014816.10 since: 2026-08-26T08:01:02Z

Publisher:
Elsevier

Published
DOI:10.1016/j.mseb.2026.119787

Terms of use:

This article is made available under terms and conditions as specified in the corresponding bibliographic description in the repository

Publisher copyright

(Article begins on next page)

07 November 2026

Materials Science and Engineering B 333 (2026) 119787

Contents lists available at ScienceDirect

Materials Science & Engineering B

journal homepage: www.elsevier.com/locate/mseb

Impulsive current test method for characterizing discharge behavior in conductive textiles

Alice Rossi [a,1], Nicolò Rimondotto [a,1], Fausto Franchini [b], Luca Ferraris [b], Luca Lavagna [a,*], Matteo Pavese [a]

[a] Polytechnic of Torino, Department of Applied Science and Technology (DISAT), C.so Duca degli Abruzzi 24, 10129 Torino, Italy
[b] Polytechnic of Torino, Department of Energy (DENERG), Viale T. Michel 5, 15121 Alessandria, Italy

ARTICLE INFO

Keywords:
Smart textiles
Impulsive current tests
Impulse current generator
Electrical resistance
Electrical discharge
Discharge current

ABSTRACT

Conductive textiles are regarded as a promising candidate for the development of both lightweight and flexible electrical components. On the other hand, the limited availability of high current electrical characterization methods poses a technological barrier which restricts the assessment of their operational limits. This study introduces a novel electrical testing method for conductive textiles and investigates the potential use of impulsive current tests for the evaluation of the current intensity leading to material damage and functional failure. The proposed methodology provides a framework for assessing the tolerance of conductive fabrics to transient high-current loads and identifying failure thresholds, thereby supporting the development and design optimization of conductive textiles for electrical protection applications, including protective garments for high-voltage environments and aerospace composite structures. Herein, each conductive fabric specimen was subjected to a set of 8/20 μs current pulses of incrementally higher energy levels. Test results suggested the identification of a correlation between samples' electrical discharge currents and their electrical resistance, providing a reliable means to estimate the discharge current of any given conductive fabric. Moreover, morphological analysis of the ablation gap conducted through Field Emission Scanning Electron Microscopy (FE-SEM) observations proposed that heating due to electrical discharge is a localized phenomenon. The findings validate impulsive current testing as an effective method for the electrical characterization of conductive textiles, thereby supporting the development of advanced smart textiles applications.

1. Introduction

In a world where electronics permeate everyday life, a key challenge lies in the integration of electronic components into textiles. Therefore, in recent years, researchers put considerable effort into identifying methods to endow fabrics with electrical conductivity, while preserving their flexibility and lightweight properties. In this context, smart textiles materials are gaining significant interest.

Conductive fabrics find utility in a wide range of applications, including stretchable sensors [1–5], flexible batteries [6–8], ELECTRICALLY HEATING TEXTILES [9–11] electromagnetic interference (EMI) shielding [12–14], antistatic devices [15,16], infrared absorption [17] and protective clothing [18–20].

Conductive textiles can be manufactured using different textiles architectures, including woven, knitted, nonwoven and fiber-reinforced composite structures, each offering specific advantages depending on the intended application. Woven fabrics are generally preferred when dimensional stability and mechanical robustness are required, whereas knitted conductive textiles provide enhanced flexibility and stretchability for wearable electronics. Nonwoven conductive fabrics offer lightweight and highly porous conductive networks suitable for multifunctional sensing and electromagnetic shielding, while carbon fiber-based textile composites have attracted increasing interest for structural multifunctional applications requiring high electrical conductivity and mechanical performance [21–23].

Electrically conductive fabrics can be created by (i) incorporating metallic wires during the weaving process, (ii) implementing electro-conductive paths using sewing or embroidery methods and (iii) by performing surface treatments [24,25].

Metallic filaments, typically made of silver, stainless steel, nickel,

* Corresponding author.
E-mail address: luca.lavagna@polito.it (L. Lavagna).
[1] Alice Rossi and Nicolò Rimondotto have contributed equally to the work.

https://doi.org/10.1016/j.mseb.2026.119787
Received 17 June 2026; Received in revised form 6 August 2026; Accepted 13 August 2026
Available online 18 August 2026
0921-5107/© 2026 The Authors. Published by Elsevier B.V. This is an open access article under the CC BY license (http://creativecommons.org/licenses/by/4.0/).

Table 1
Main characteristics of the commercial conductive fabric samples.

Sample	Fabric substrate	Weave pattern	Coating	Additives	Fabric thickness [mm]	Coated fabric weight [g/m^2]
A1	PET	Ripstop	Cu - Ni	–	0.135	100–120
B1	PA	Ripstop	Cu - Ni	–	0.1	75
B2	PA	Ripstop	Cu - Ni	Flame retardant UL94 V0	0.2	240
B3	PET	Taffeta	Cu - Ni	Flame retardant UL94 V0	0.2	240
C1	PET	Ripstop	Cu - Ni	–	0.09	80
C2	PA	Ripstop	Ag - Cu - Ni	–	0.125	110
C3	PET	Ripstop	Cu - Sn	–	0.10	120
C4	PA	Ripstop	Cu - Ag	–	0.11	85
C5	PA	Ripstop	Ag - Cu - Sn	–	0.12	81
C6	PA	Ripstop	Ag	–	0.090	43
C7	PA	Ripstop	Ag	Conductive Polyurethane	0.10	58

aluminum and copper, can be added into the textile structure to provide electrical conductivity. However, some metals corrode easily, are difficult to process and reduce flexibility and lightness [26]. These aspects have guided research towards the development of alternative solutions, such as conductive polymer yarns (CPYs).

CPYs can be divided into two categories, namely bulk CPYs and surface CPYs. While the former include intrinsically CPYs, polymer yarns combined with metallic filaments or loaded with conductive additives, the latter consist of polymeric fibers coated with conductive layers, i.e., metals, conductive polymers, carbon nanotubes or carbon black [27].

An alternative approach involves the deposition of conductive coatings on fabric substrates, through processes such as printing of metallic inks, electroless plating, electrochemical deposition, physical or chemical vapor-phase deposition and spray coating. The process selection is dictated by different parameters, i.e., operating temperatures, substrate and coating type and target application which includes coating thickness requirements.

Printing techniques allow the local and direct deposition of conductive ink and the patterning of conductive pathways on different types of substrates at ambient conditions [24]. Both electroless and electrochemical deposition methods guarantee coherent metal deposition, industrial scalability and can be performed on complex-shaped substrates [28,29]. Vapor-phase deposition processes produce a broad variety of coatings with different thicknesses to achieve varying conductivity levels [30]. Finally, spray coating is a well-established technique for the deposition of uniform and adherent coatings on irregular substrates like fabrics [31].

Although electrical conductivity is commonly characterized through static parameters such as surface resistance, volume resistivity and sheet resistance [32], these measurements are generally performed under low-current steady-state conditions. Such conventional characterization methods provide valuable information on the initial electrical properties of conductive textiles but do not assess their ability to withstand high-current transient events. During impulsive electrical loading, the conductive network may undergo rapid joule heating, localized melting, coating delamination, fiber degradation or irreversible changes in electrical performance, phenomena that cannot be predicted from conventional low-current measurements alone.

High-current impulsive events may occur in several practical scenarios, including lightning-induced currents, arc-flash accidents, electrical faults, short-circuit events and transient overcurrent conditions affecting protective garments, conductive composites and technical textiles employed in aerospace. In these situations, conductive textiles must preserve both their electrical functionality and structural integrity under extremely short-duration current pulses.

In this context, few studies have addressed the behavior of conductive fabrics under high-intensity current exposure. In this regard, it is worth citing the research work conducted by Cristancho et al. [33–35] which focuses on the simulation of lightning discharge using pulses of fixed current intensity and varying waveforms, i.e., 4/10 μs, 8/20 μs, 10/350 μs.

Herein, a novel approach is proposed to investigate conductive fabrics' operational limits by performing tests using 8/20 μs pulses at incrementally higher energy levels. These tests are accordingly designed to identify critical current values leading to the functional failure of the material. The novelty of the present work lies not only in the development of an impulsive current characterization methodology for conductive textiles, but also in the identification of a predictive correlation between the initial electrical resistance of a conductive fabric and the discharge current corresponding to its electrical damage threshold. This relationship provides a practical tool for estimating the current tolerance of conductive textiles through a simple resistance measurement, thereby reducing the need for extensive impulsive-current testing during the preliminary assessment of new materials.

The proposed methodology can support the development of conductive textiles for electrical protection applications, including protective garments based on the Faraday cage principle for personnel working in high-voltage environments, as well as aerospace composite structures. By enabling the evaluation of the tolerance to transient high-current loads and the identification of failure thresholds, the method provides valuable information for material selection and design optimization.

2. Experimental section

2.1. Conductive fabric test samples

The impulsive current tests were performed on Conductive fabrics selected to represent a broad range of commercially available metallized textiles for technical applications, including emi shielding, electrical protection and lightweight conductive structures. The selected materials cover different textile substrates (polyamide and polyester), weave architectures and metallic coating compositions (Ag, Cu, Ni and Sn), allowing the influence of these parameters on transient high current tolerance to be investigated. Commercial samples, whose main characteristics are shown in Table 1, were purchased from *Ghiringhelli EMI Shielding Products* (Italy), *Euro Technologies* (Italy) and *Shieldex* (Germany). LABORATORY-SCALE SPECIMENS, discussed in Section 3.6, were obtained via electrochemical copper deposition process performed on polyamide (PA) and polyester (PET) plain weave fabrics, on which activation and electroless copper deposition were previously carried out. Polyamide and polyester fabrics were selected as substrates owing to their widespread use in technical and protective textile applications, making them representative materials for the assessment of conductive textile systems. For each fabric type four 5 × 1 cm samples were obtained.

Surface morphology of the samples subjected to impulsive current tests was investigated through a Leica stereomicroscope and a *Merlin-Zeiss* Field Emission Scanning Electron Microscope (FE-SEM). FE-SEM images were taken on previously platinum sputtered samples. Thermogravimetric Analysis (TGA) was conducted by means of a TGA

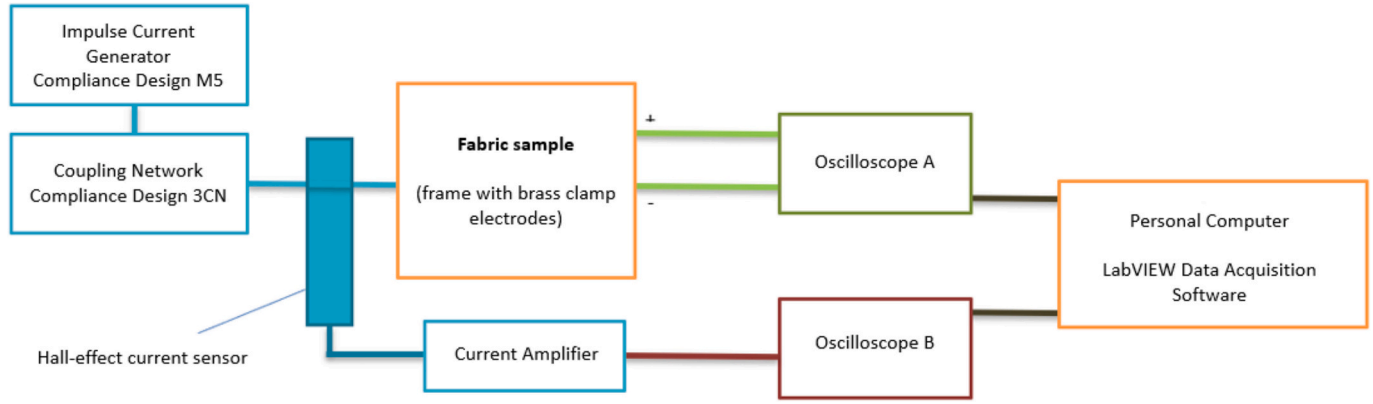


Fig. 1. Impulsive current bench test configuration.

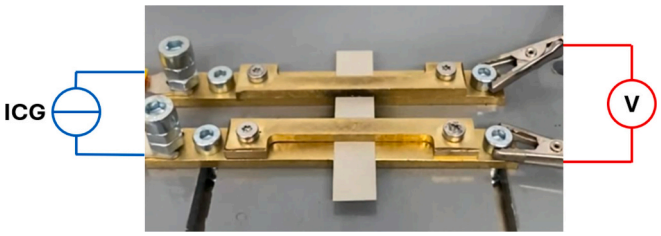


Fig. 2. Voltage measurement points.

instrument *Mettler Toledo* in order to determine the metal fraction of the commercial conductive fabric samples.

2.2. Bench test configuration

Impulsive current tests allowed the determination of the current intensity causing material damage and the degradation in the functional performance. The above-mentioned test configuration is shown in Fig. 1, and it is mainly composed of an Impulse Current Generator (ICG) *Compliance Design M5* combined with a coupling network *Compliance Design 3CN*. The ICG ensures the delivery of 8/20 μs high-energy current pulses with an adjustable voltage ranging from 10 V to 6 kV, according to the IEC 61000–4-5 standard [36]. The high energy pulses were conducted to the samples through connecting cables and brass electrodes, ensuring both mechanical support and electrical connection. To minimize measurement artifacts associated with the electrical contacts, all specimens were tested using the same brass electrodes, identical contact area and constant clamping configuration throughout the experimental campaign. The electrical connections were maintained unchanged for all measurements, ensuring repeatable interface conditions and minimizing the influence of contact resistance on the impulsive current measurements. Contact resistance is recognized as a potential source of uncertainty in electrical characterization, particularly for low-current resistance measurements as discussed by tang et al. [37]. however, in the present work, the investigated electrical quantities were obtained under impulsive high-current conditions, where the measurements are dominated by the discharge event rather than by the contact interface.

Current measurements were carried out through a Hall-effect current sensor *Tektronix A6303* powered by a Current Amplifier *Tektronix AM 503*. Voltage was recorded through a two-channel oscilloscope *GW Instek GDS-2062*, aimed to perform differential measurements.

The voltage was measured directly between the two electrodes holding the textile specimen (Fig. 2), thus corresponding to the total voltage drop across the sample. The current signal is fed to a second oscilloscope, which also communicates with LabVIEW Data Acquisition Software. Time synchronization is implemented using a second current probe, connected in parallel to the oscilloscopes' auxiliary inputs.

Material behavior was assessed by testing four 5 × 1 cm samples for each fabric type, which was considered sufficient to capture the variability among samples and obtain representative mean values.

Samples were placed between the electrodes so that only a central 1 × 1 cm area was stressed during characterization. Preliminary testing was carried out on the first sample by gradually increasing the ICG voltage, with steps ranging from 50 to 250 V, in order to determine the critical ICG voltage triggering electrical discharge and functionality loss (Fig. 3).

The remaining samples were characterized by operating current pulses around the previously determined critical ICG voltage value. This procedure guarantees an accurate and consistent evaluation of the fabrics' behavior together with the assessment of current and voltage values responsible for electrical discharge.

Power P and energy E involved during electrical discharges were estimated from voltage V and current I signals by means of Eqs. (1) and (2) respectively

$$P = V \bullet I \tag{1}$$

$$E = \int_{t_{on}}^{t_{off}} P(t)\, dt \tag{2}$$

where t_{on} and t_{off} are pulse onset and offset times.

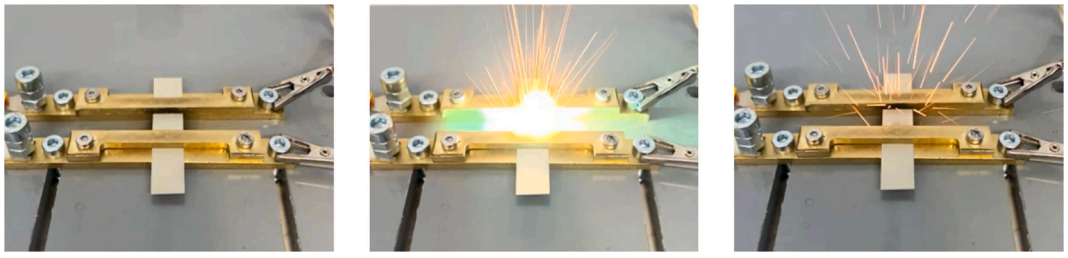


Fig. 3. Electrical discharge induced on sample C3.

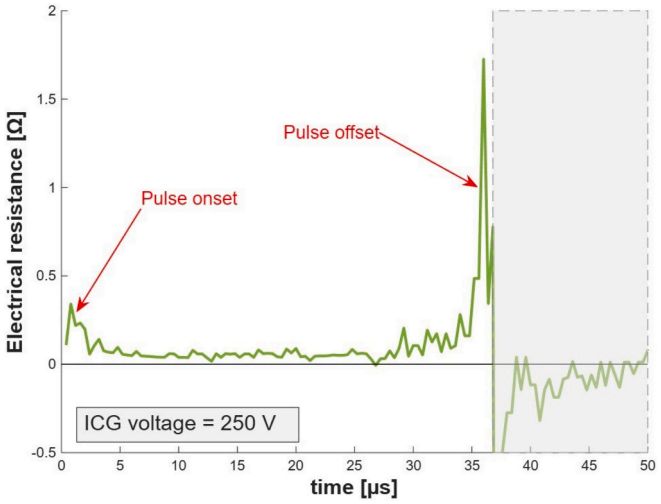


Fig. 4. Electrical resistance plot for sample B2. The shaded area refers to time intervals following the end of the pulse.

Table 2
Electrical resistance of the samples: measured values (with standard deviation) and manufacturer's stated value.

Sample	Measured mean initial electrical resistance [Ω]	Stated electrical resistance [Ω]
A1	0.236 ± 0.092	< 0.05–0.08
B1	0.083 ± 0.004	< 0.07
B2	0.054 ± 0.003	< 0.07
B3	0.072 ± 0.001	< 0.07
C1	0.075 ± 0.004	< 0.05
C2	0.017 ± 0.002	< 0.009
C3	0.021 ± 0.001	< 0.02
C4	0.040 ± 0.005	≤ 0.03
C5	0.029 ± 0.002	< 0.02
C6	0.316 ± 0.009	< 0.3
C7	0.422 ± 0.160	< 0.3

The resistance R of the samples was assessed through a non-destructive pulse, setting an ICG voltage of 250 V, according to Eq. (3).

$$R = \frac{V}{I} \tag{3}$$

Given the thermal diffusivity of copper, the main metal in the analyzed fabric coatings, it can be stated that the heating induced by the electrical discharge is a highly localized phenomenon. More precisely, by considering heat propagation governed by conduction only, the thermal diffusion length within the region under test is approximately 50 μm over 25 μs. This suggests that heat remains confined in the affected region rather than propagating across the entire sample.

The maximum local temperature T_{max} reached during electrical discharge was thus roughly estimated applying Eq. (4), assuming in-plane heat conduction and neglecting radiation,

$$T_{max} = T_{amb} + \frac{E}{C} \tag{4}$$

where T_{amb} corresponds to the room temperature and C to the thermal capacity of the samples, defined as the product between the mass of the metal-coated fabric and the metal's specific heat capacity.

3. Results and discussion

3.1. Evaluation of the initial electrical resistance of the fabric samples

The electrical resistance of the fabric samples was evaluated by means of low energy pulses in order to prevent damage. More specifically, the ICG voltage was set to 250 V and for each material type four measurements were performed to obtain an average value. The electrical resistance plots were obtained from the current and voltage signals using Eq. (3). As an example, Fig. 4 shows the resistance plot for sample B2. For each sample the resistance value, reported in Table 2, was determined as the arithmetic mean of the datapoints within the valley of the plot. For some samples, resistance values higher than those stated by the manufacturer were recorded. This deviation may be attributed to surface oxidation of the conductive coating, which can increase contact resistance and reduce the effective electrical conductivity of the material.

3.2. Assessment of electrical discharge conditions

For each fabric type, the critical ICG voltage value triggering electrical discharge was obtained by performing several impulsive current tests at progressively higher energy levels. The recorded maximum current and voltage values can be therefore plotted as a function of the set ICG voltage.

As an example, Fig. 5 shows the above-mentioned plots for sample B2, for which the electrical discharge was triggered by setting an ICG voltage of 1650 V. The maximum current plot shows a linear increase with ICG voltage, while the same trend does not apply to the maximum voltage plot. In this case a steep increase can be observed at electrical

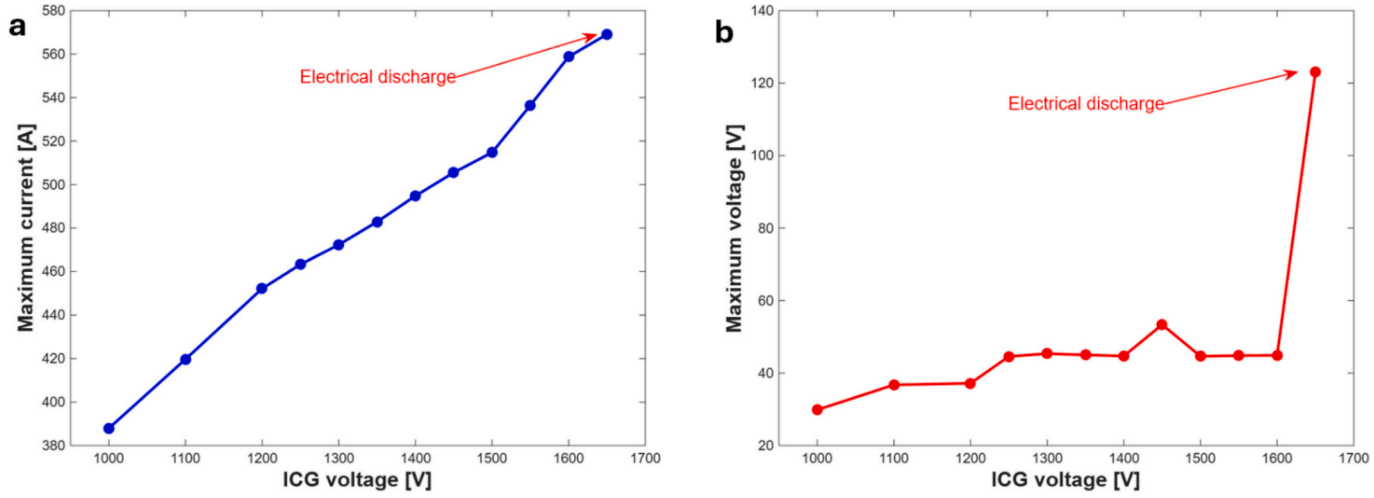


Fig. 5. a Maximum current vs ICG voltage plot for sample B2. b Maximum voltage vs ICG voltage plot for sample B2.

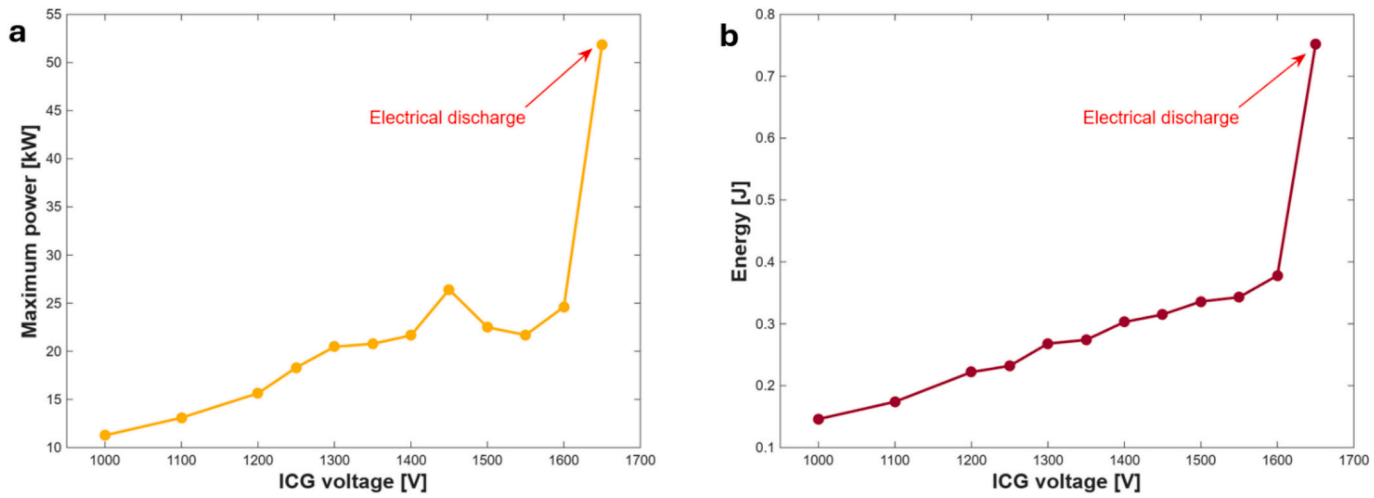


Fig. 6. a Maximum power vs ICG voltage plot for sample B2. b Energy vs ICG voltage (b) plots for sample B2.

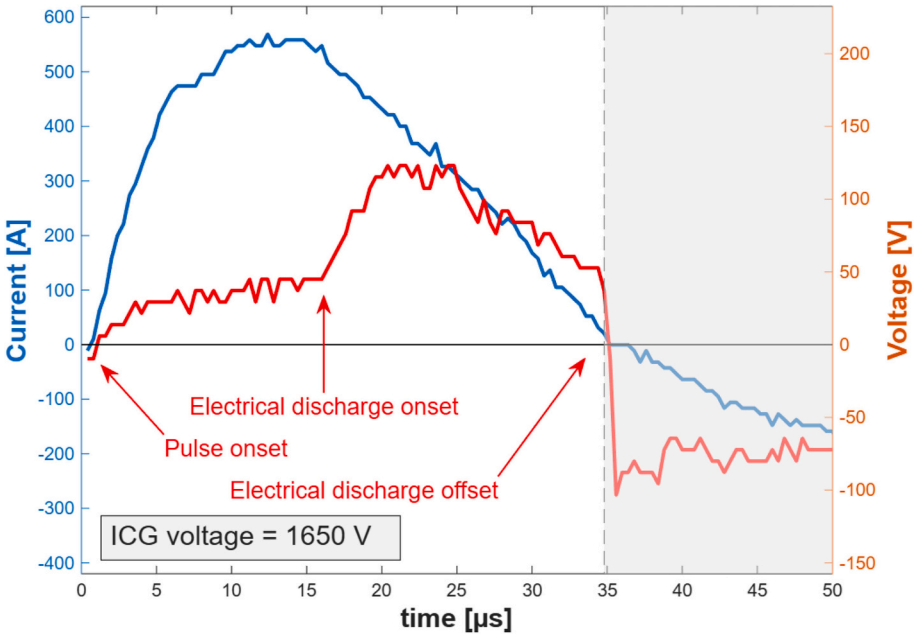


Fig. 7. Current and voltage signals at electrical discharge for sample B2. The shaded area refers to time intervals following the end of the pulse.

discharge.

It should be noted that the damaging of the sample's coating causes the air-gap discharge to be the actual conductive element of the circuit. The electric arc resulting from high current availability is characterized by an electrical resistance higher than that of the sample, thus explaining the voltage peak.

As far as maximum power and energy are concerned, their values were calculated applying Eqs. (1) and (2), based on the maximum current and voltage signals. With respect to sample B2 (Fig. 6), values of 52 kW and 0.75 J for power and energy respectively were found to induce electrical discharge.

3.3. *Investigation of the electrical discharge mechanism*

In order to assess discharge behavior of every conductive fabric type, three samples each were tested delivering pulses obtained by setting the ICG at the previously detected critical value. As an example, Fig. 7 shows current and voltage waveforms for sample B2. It can be noted that the measured current replicates the pulse shape, which appears to be asymmetric and characterized by a rise time ranging between 10 and 15 µs and by a time to decay to one-half peak value of approximately 25 µs. The pulse offset time is equal to 35 µs, being the point where the current signal drops to 0 A. The subsequently recorded negative values are due to instrumental artifacts and are irrelevant for test purposes.

The current waveform does not provide an indication of circuit opening (corresponding to sample damaging), since the current continues to flow across the electrical discharge established between the electrodes. On the other hand, the voltage measured directly across the sample exhibits two distinct step-like variations. Before failure, the measured voltage corresponds to the drop across the conductive fabric. Once the coating is perforated and an electrical discharge is established, the measured voltage corresponds to the electrode-to-electrode voltage sustained by the discharge channel. The increase in voltage observed at the onset of the discharge should therefore not be interpreted as the steady-state arc voltage alone. Rather, it reflects the transient redistribution of the voltage immediately following sample perforation and is influenced by the dynamic response of the pulsed discharge circuit, including parasitic inductive effects during the rapid current variation.

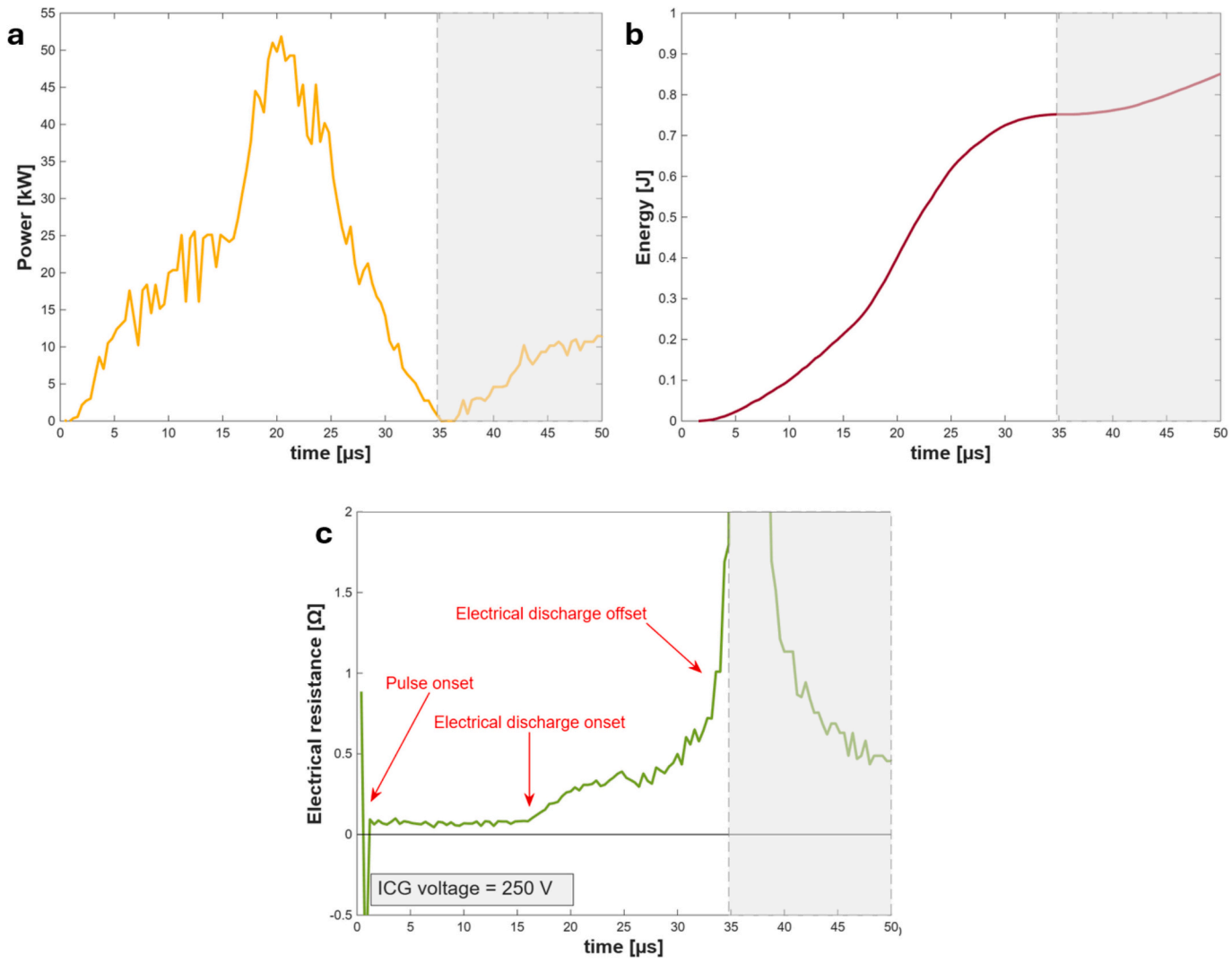


Fig. 8. a) Power plot at electrical discharge for sample B2. b) Energy plot at electrical discharge for sample B2. c) Resistance plot at electrical discharge for sample B2.

Based on current and voltage signals recorded during electrical discharge, it is possible to obtain power, energy, as well as electrical resistance plots, shown in Fig. 8 for sample B2. The resistance signal shows an initial region with nearly constant behavior corresponding to the sample resistance, followed by an upward-sloping segment related to the parallel between the damaged sample and the electrical arc.

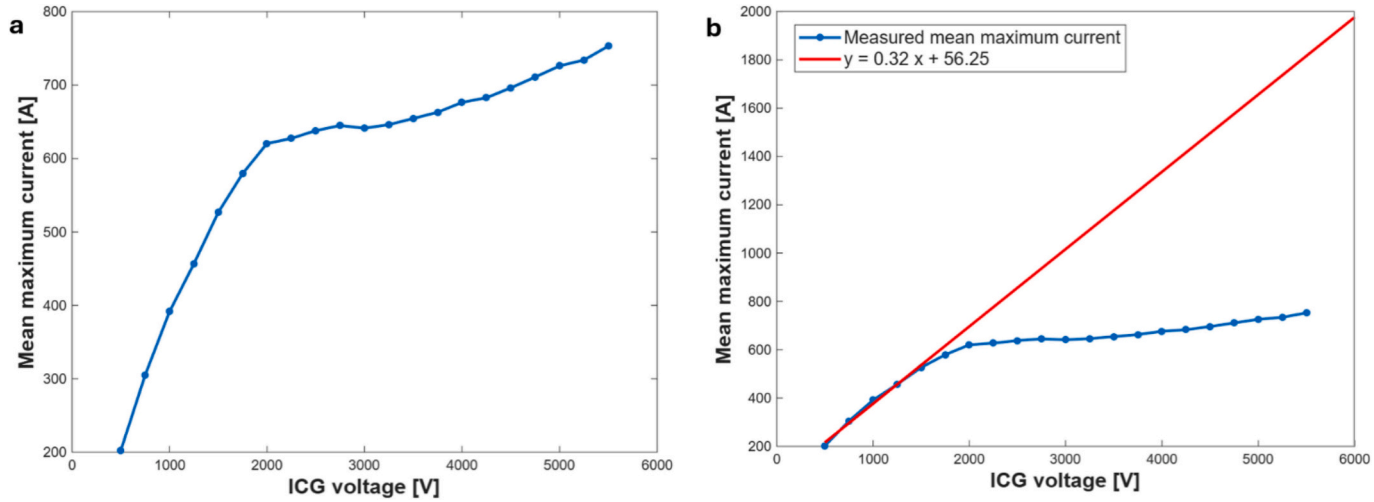


Fig. 9. a) Mean maximum current vs ICG voltage plot. b) linear interpolation.

Table 3
Outcomes of the impulsive current tests performed at electrical discharge conditions.

Sample	Mean maximum measured current [A]	Fitted theoretical maximum current [A]	Mean maximum voltage [V]	Mean maximum power [kW]	Mean energy [J]
A1	374 ± 30	384	118 ± 15	42 ± 8	0.79 ± 0.14
B1	400 ± 8	400	112 ± 43	35 ± 13	0.58 ± 0.20
B2	563 ± 34	584	128 ± 62	57 ± 23	0.86 ± 0.33
B3	440 ± 6	451	81 ± 5	35 ± 2	0.61 ± 0.04
C1	338 ± 17	329	70 ± 16	20 ± 5	0.31 ± 0.11
C2	733 ± 16	1753	73 ± 25	37 ± 12	0.37 ± 0.22
C3	751 ± 13	1777	82 ± 25	46 ± 11	0.51 ± 0.24
C4	643 ± 6	941	84 ± 20	40 ± 3	0.71 ± 0.08
C5	659 ± 10	1073	72 ± 18	51 ± 26	0.91 ± 0.42
C6	176 ± 17	216	139 ± 41	22 ± 4	0.37 ± 0.07
C7	164 ± 10	208	97 ± 17	15 ± 3	0.27 ± 0.05

Current and voltage plots at electrical discharge for each material type can be found in *Supplementary Material*. Different current trends can be identified, which appear to be typical of the set ICG voltage, as illustrated by representative examples in Supplementary Material Fig. S1 and Fig. S5. More precisely, when the ICG voltage is set at values lower than 2000 V (Supplementary Material Fig. S1) the current signal reproduces the pulse shape. Greater values determine, by contrast, the occurrence of a truncation of the main peak and of a local maximum at times subsequent to pulse termination (Supplementary Material Fig. S5). While the former is due to instrumental limitations, the latter can be explained considering the presence of stray inductance in the ICG coupling network instead. The coupling network consists of capacitors and resistors designed to generate standardized impulse waveforms. Whenever the sample does not conduct linearly, these components can release energy at times subsequent to the main pulse.

The voltage signal exhibits step-like behavior only during sudden sample breakdown, as observed for samples B2 (Supplementary Material Fig. S3) and C6 (Supplementary Material Fig. S9). A drift or a saturated response (Supplementary Material Fig. S8) can be referred to the rapid heating of the sample instead, causing an increase of electrical resistance.

A more detailed analysis of the main peak truncation is derived by examining the plot obtained from the mean maximum current values recorded for each sample as a function of the ICG voltage (Fig. 9a). While for set ICG voltage lower than 2000 V the current signal increases linearly with the applied voltage, for greater values a saturation in the current signal can be noted since the sensor's instrumental limit was reached.

A reasonable estimate of the effective current to which a sample is subjected can be made by assuming that the current increases linearly also when applying ICG voltage values higher than 2000 V. This assumption is plausible considering that the maximum current which can be delivered by the ICG is expected to be 3000 A. The obtained fit, shown in Fig. 9b, allows the estimation of the fitted theoretical maximum current flowing across the samples, thereby overcoming the limitations imposed by the saturation of the current probe. The theoretical maximum current values are reported in Table 3 together with the measured average maximum current, voltage, power and energy.

Experimental data show that samples C2 and C3 experienced the highest values of both measured and fitted current, yet were characterized by the lowest voltages. This aspect can be explained considering that the voltage across the sample was recorded through a two-channel oscilloscope, which performs a differential measurement. Therefore, a decrease in the sample's resistance leads to a loss of voltage signal resolution, since the measured differential voltage becomes negligible.

Although impulsive current signals exhibit a broad frequency spectrum, the present analysis assumes that conductive textiles behave predominantly as a resistive element during the short-duration current pulse. This assumption is justified by the limited dimensions of the tested specimens and by the fact that the investigated degradation mechanisms are mainly governed by joule heating and energy dissipation rather than by wave propagation phenomena. Consequently, the initial electrical resistance represents an appropriate parameter for correlating the electrical loading with the observed material degradation.

By plotting both the measured (Fig. 10a) and fitted theoretical maximum current (Fig. 10b) as a function of the electrical resistance of the samples, a correlation between the physical quantities can be identified. Hyperbolic interpolations performed on measured and fitted datasets enable the estimation of the current triggering electrical discharge once the resistance of any given conductive fabric is known.

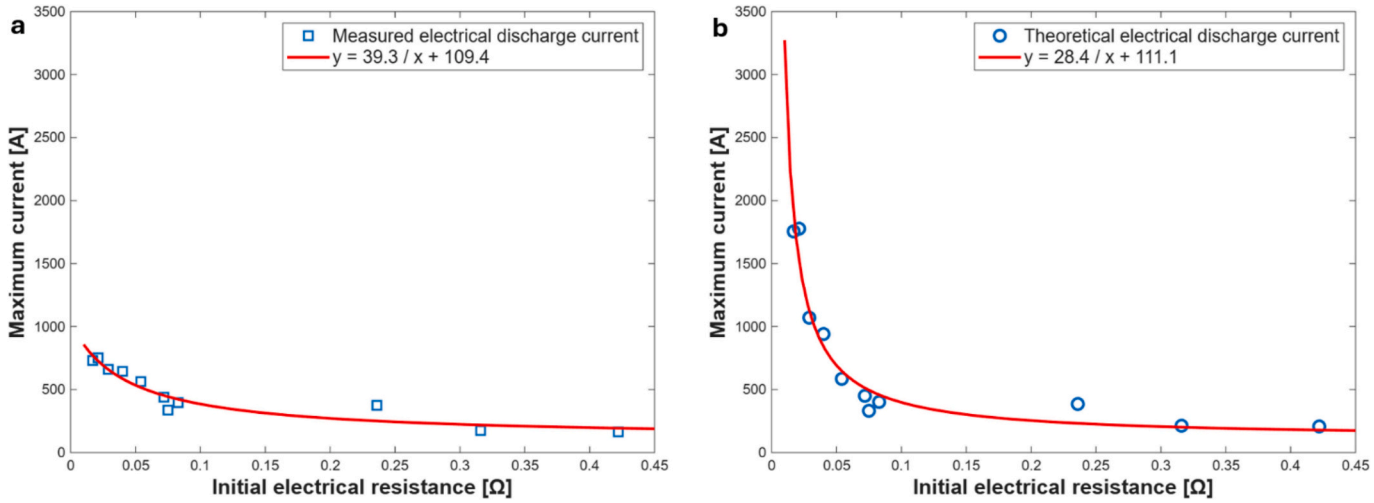


Fig. 10. a) Correlation between the samples' electrical resistance and the measured current. b) Correlation between the samples' electrical resistance and the fitted maximum current.

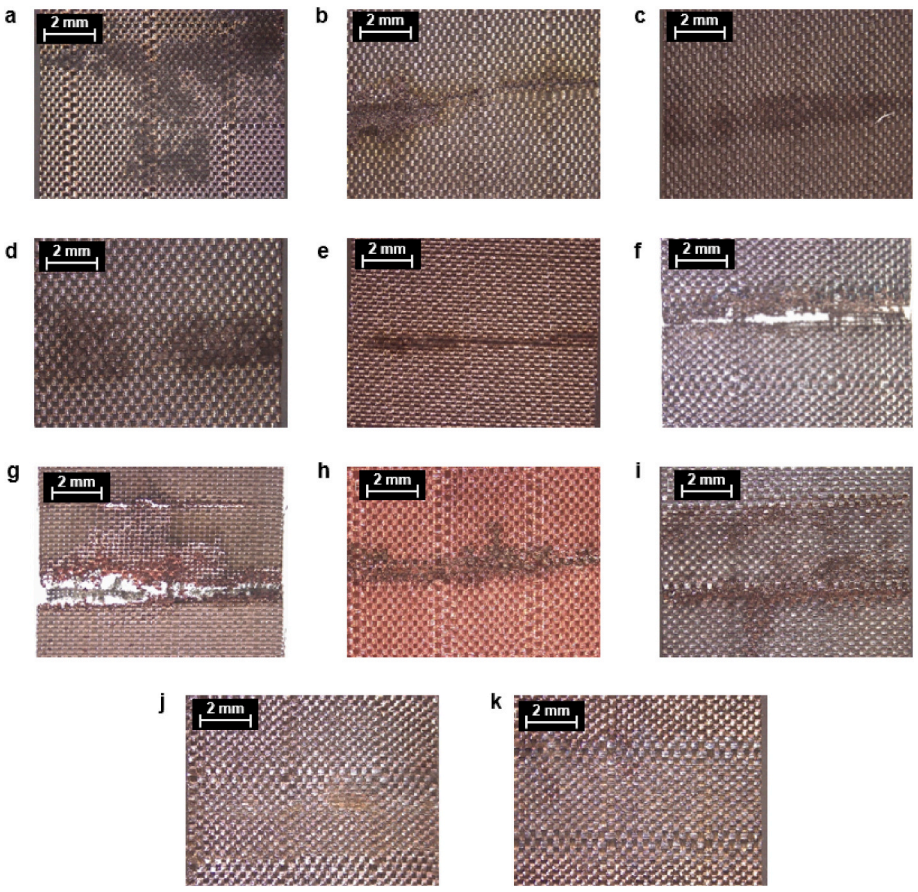


Fig. 11. Gap caused by electrical discharge for sample a) A1, b) B1, c) B2, d) B3, e) C1, f) C2, g) C3, h) C4, i) C5, j) C6 and k) C7.

Table 4
Estimated maximum local temperatures for polyester (PET) and polyamide (PA) coated fabrics.

Sample	Fabric substrate and metal coating	T_{HAZ} [°C]	T_{gap} [°C]	I_D
A1	PET ripstop Cu Ni	201	1280	0
B1	PA ripstop Cu Ni	215	2203	1
B2	PA ripstop Cu Ni	113	818	0
B3	PET taffeta Cu Ni	87	342	0
C1	PET ripstop Cu Ni	124	3021	1
C2	PA ripstop Ag Cu Ni	116	2319	1
C3	PET ripstop Cu Sn	138	1797	0
C4	PA ripstop Cu Ag	256	3091	1
C5	PA ripstop Ag Cu Sn	349	1016	0
C6	PA ripstop Ag	390	1595	0
C7	PA ripstop Ag	228	542	0

As far as the fit carried out on the measured current is concerned, the observed hyperbola flattening is attributable to the saturation of the current signal.

3.4. Assessment of the temperatures reached during electrical discharge

The maximum local temperature reached in each fabric during electrical discharge was estimated using Eq. (4) following two approaches: (i) assuming that heat-affected zone coincides with the area of the sample comprised between the electrodes, equal to 1 cm^2, yielding T_{HAZ} and (ii) considering the ablation gap area only, yielding T_{gap}.

The ablation gap area was determined from stereomicroscope images (Fig. 11), with a significant degree of uncertainty. For each sample a damage identifiability parameter I_D was defined, with a value equal to 1 when the damaged zone can be unambiguously identified and 0 otherwise. The identifiability parameter together with the estimated maximum local temperatures, are reported in Table 4.

Calculations account for the combined mass of the fabric and metal coating, assuming that heat transfer occurs via in-plane conduction and predominantly out-of-plane radiation. As radiation is not strictly confined to the normal direction, the reported temperatures are likely overestimated.

For the computation performed at I_D equal to 1, the resulting T_{gap} appears sufficient to induce melting of the metallic alloy constituting the samples' coating within the ablation gap.

It should be emphasized that the calculated temperatures are intended as approximate estimates rather than exact values. The proposed model is based on several simplifying assumptions, including uniform energy distribution within the selected heat-affected region, homogeneous material properties, negligible heat losses during the impulse duration except for simplified conductive and radiative contributions, and complete conversion of the dissipated electrical into heat. Furthermore, the actual geometry of the damaged region is irregular and only approximately represented by the measured ablation gap area, introducing additional uncertainty. Consequently, the calculated temperatures should be interpreted primarily as order-of-magnitude estimates, useful for assessing whether the temperatures reached during the discharge are compatible with the melting or degradation of the conductive coating, rather than as precise measurements of the local peak temperature.

3.5. Quantification of the metallic fraction in the textiles

The metallic fraction of the conductive textiles was determined by thermogravimetric analysis. Figs. 12 and 13 show thermogravimetric curves for polyamide (PA) and polyester (PET) uncoated fabrics and for

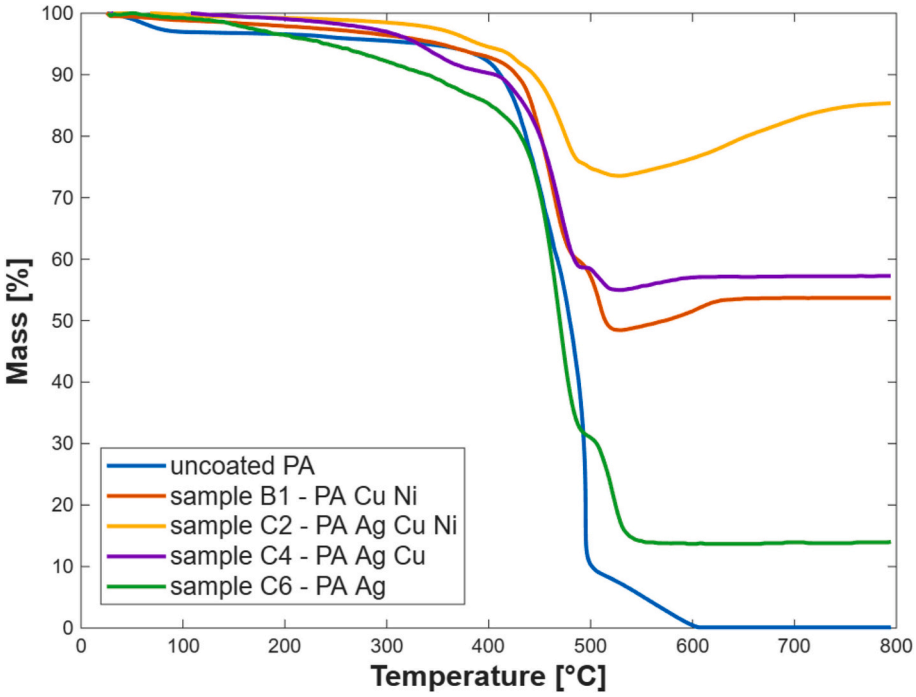


Fig. 12. Thermogravimetric curves for uncoated PA and for samples B1, C2, C4 and C6.

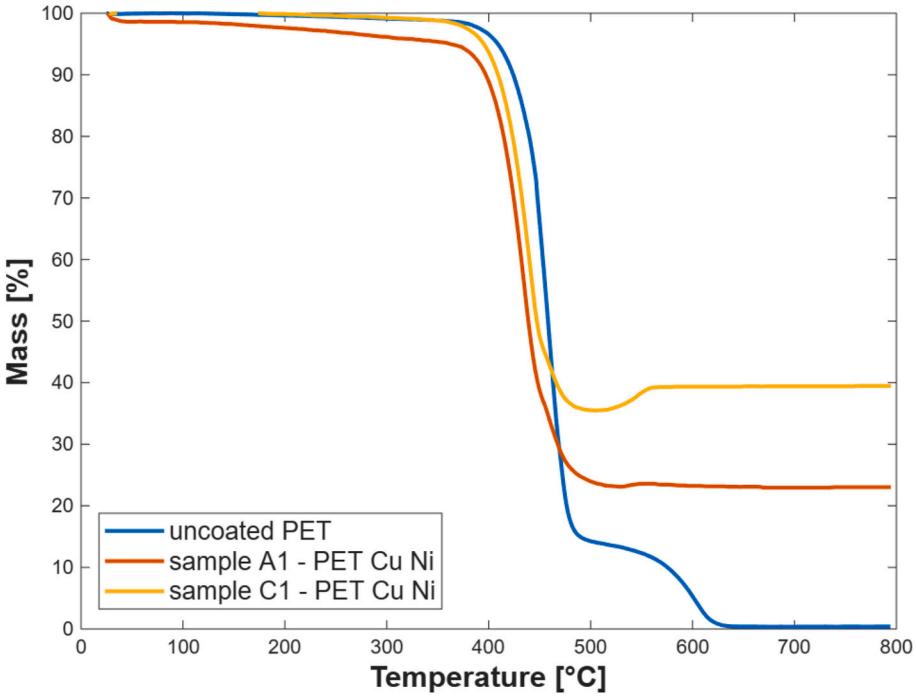


Fig. 13. Thermogravimetric curves for uncoated PET and for samples A1 and C1.

Table 5
Mass fractions of the analyzed metallic coatings.

Sample	Fabric substrate	Metallic coating	Coating mass fraction [%]
A1	PET	Cu - Ni	23.1
B1	PA	Cu - Ni	48.5
C1	PET	Cu - Ni	35.5
C2	PA	Ag - Cu - Ni	73.6
C4	PA	Ag - Cu	55.0
C6	PA	Ag	13.7

Table 6
Electrical resistance of laboratory scale-prepared samples.

Sample	Mean initial electrical resistance [Ω]
PET – electroplating 15 min	0.019 ± 0.003
PET – electroplating 30 min	0.016 ± 0.001
Cordura® - electroplating 15 min	0.013 ± 0.004
Cordura® - electroplating 30 min	0.010 ± 0.001

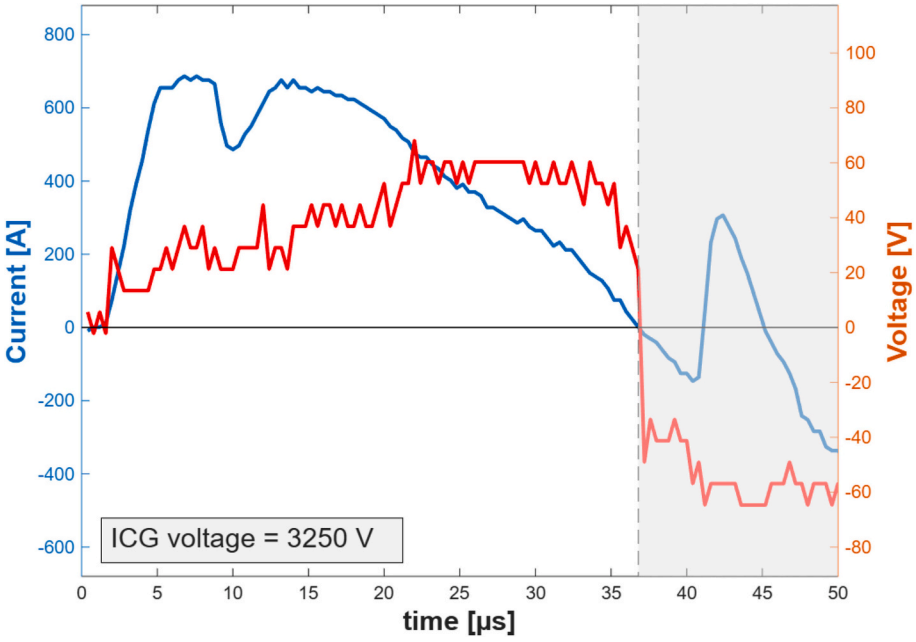


Fig. 14. Current and voltage signals at electrical discharge for sample PET - 15 min electroplating.

Table 7
Estimated discharge current values for fabric sample produced at laboratory scale.

Sample	Estimated discharge current [A]
PET – 30 min electroplating	1886
PA – 15 min electroplating	2296
PA – 30 min electroplating	2951

samples A1, B1, C1, C2, C4 and C6. The curves on uncoated fabrics show the absence of residue, while the curves made on conductive fabrics exhibit a minimum which corresponds to the metallic coating's mass, listed in Table 5. As far as samples A1, B1, C1, C2 and C4 are concerned, a subsequent upward trend can be noted, ascribable to oxide formation at high temperatures.

3.6. Laboratory-scale samples

Impulsive current tests were also performed on laboratory scale-prepared samples, which were obtained via an electrochemical copper deposition process. As far as electrical resistance is concerned, the measured values are listed in Table 6 and appear to be among the lowest.

Impulsive current tests suggested that the only sample experiencing electrical discharge was PET – 15 min electroplating. Fig. 14 displays the corresponding current and voltage signals where voltage step-like behavior denotes, once again, the sample's damaging during electrical discharge. The recorded values are 682 ± 7 A and 1057 A for the mean maximum measured current and the fitted theoretical maximum current respectively. The estimate of the maximum local temperature reached during electrical discharge resulted in a value of 1020 °C.

The remaining laboratory scale prepared samples, i.e., PET – 30 min

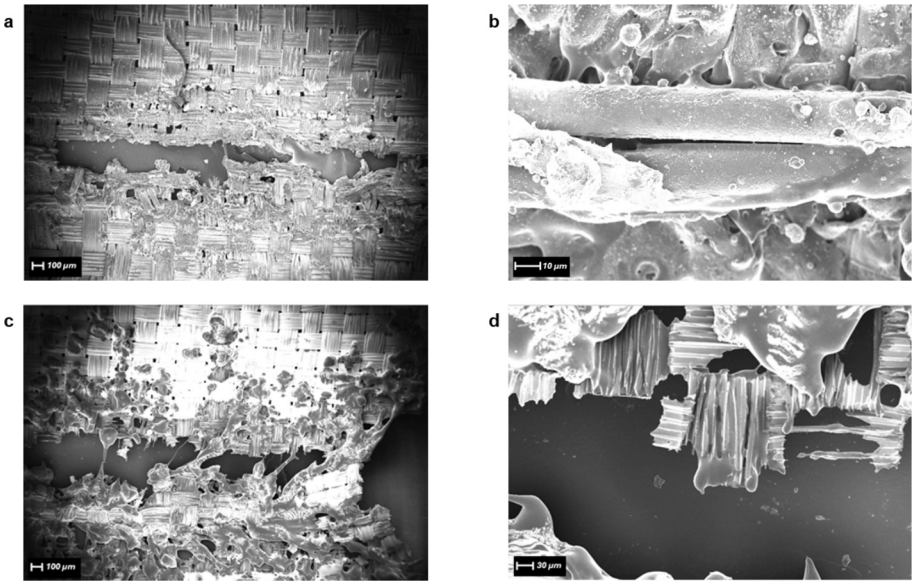


Fig. 15. a), b) FE-SEM images of sample C2 after impulsive current tests. c), d) FE-SEM images of sample C3 after impulsive current tests.

and PA – 15 and 30 min electroplating, were not affected by any electrical discharge since the available ICG was unable to produce pulses of sufficient energy. Based on the relationship identified in Fig. 10b the corresponding discharge currents can be estimated and their values are listed in Table 7.

The same correlation was employed for the estimation of the discharge current of sample PET – 15 min electroplating, for which a value of 1606 A was obtained. The assessed value exceeds the actual discharge current, and the discrepancy can be explained assuming the presence of defects in the laboratory-scale coating.

3.7. Surface morphology

FE-SEM observations were carried out on the conductive fabric samples that endured the highest currents, i.e., samples C2 and C3, to examine their morphological features. Fig. 15a and c reveal the complete lack of material in the area affected by electrical discharge, suggesting possible vaporization of the metallic coating. In particular, an ablation pattern can be noted, which appears to be parallel to the electrodes and perpendicular to the current flow [33]. The localized nature of the damage can be explained considering the reduced heat diffusion length of the copper-based coating.

Moreover, the areas surrounding the ablation pattern are characterized by the presence of agglomerates indicating polymeric fibers' rapid melting and solidification. As displayed in Fig. 15b and d, impulsive current tests led to a loss of support provided by the polymeric fibers to the metallic coating. This behavior can be explained assuming that the temperatures reached in the regions adjacent to the ablation gap were sufficient to cause the melting of the polymer while not affecting the metallic coating.

4. Conclusions

This study aims to provide an electrical characterization of commercially available conductive fabrics and explores the potential application of impulsive current tests for the assessment of the current intensity causing material damage and functional failure.

Discharge behavior of each conductive fabric type was investigated by performing several impulsive current tests at incrementally higher energy levels, aimed to determine the critical ICG voltage triggering electrical discharge.

Testing revealed a step-like behavior of the voltage signal, typical of the sample's failure process. Instead, the current waveform does not provide an indication of circuit opening. However, different current trends can be identified and are found to be characteristic of the applied ICG voltage. More specifically, for ICG voltage values lower than 2000 V the current signal conforms to the pulse shape, whereas increased values determine the occurrence of a truncation of the main peak. This effect is attributable to the saturation of the current signal, resulting from instrumental limitation. Beyond the validation of the proposed testing methodology, the present study demonstrates that the initial electrical resistance of conductive textiles can be used as a predictive parameter for estimating the discharge current associated with electrical failure. This finding represents a practical design tool for the rapid screening of conductive textiles intended for applications involving transient high current events.

Moreover, an estimate of the maximum local temperatures reached by the samples suggests that melting of the metallic coating occurs only within the ablation gap induced by the electrical discharge.

Finally, FE-SEM observations confirm the localized nature of the heating phenomenon, as in the regions adjacent to the ablation gap the temperatures reached are sufficient to melt the polymer fibers, but not high enough to induce melting of the metallic coating.

Overall, the conducted study validates impulsive current testing as an effective method for the electrical characterization of conductive fabrics, allowing the assessment of discharge behavior as well as critical current thresholds, while contributing to the development and characterization of high-performance protective textiles.

CRediT authorship contribution statement

Alice Rossi: Writing – original draft, Visualization, Validation, Methodology, Investigation, Data curation, Conceptualization. **Nicolò Rimondotto:** Writing – original draft, Visualization, Validation, Methodology, Investigation, Data curation, Conceptualization. **Fausto Franchini:** Writing – review & editing, Validation, Software, Resources, Investigation. **Luca Ferraris:** Supervision, Software, Resources, Project administration. **Luca Lavagna:** Writing – review & editing, Writing – original draft, Investigation. **Matteo Pavese:** Writing – review & editing, Validation, Supervision, Project administration, Methodology, Funding acquisition.

Funding

The authors did not receive support from any organization for the submitted work.

Declaration of competing interest

The authors declare that they have no known competing financial interests or personal relationships that could have appeared to influence the work reported in this paper.

Appendix A. Supplementary data

Supplementary data to this article can be found online at https://doi.org/10.1016/j.mseb.2026.119787.

Data availability

Data will be made available on request.

References

[1] G. Gamberini, S. Tognarelli, A. Menciassi, Soft conductive textile sensors: characterization methodology and behavioral analysis, Sensors (2025), https://doi.org/10.3390/s25144448.
[2] Y. Pan, C. Yang, Z. Du, J. Xue, G. Jin, H. Mou, Highly stretchable and sensitive sensing composite yarn based on multidimensional structure modulation for wearable E-textiles, Appl. Mater. Today (2025), https://doi.org/10.1016/j.apmt.2025.102591.
[3] X. Guo, W. Hong, B. Hu, T. Zhang, C. Jin, X. Yao, H. Li, Z. Yan, Z. Jiao, M. Wang, B. Ye, S. Wei, Y. Xia, Q. Hong, Y. Xu, Y. Zhao, Human touch sensation-inspired, ultrawide-sensing-range, and high-robustness flexible piezoresistive sensor based on CB/MXene/SR/fiber nanocomposites for wearable electronics, Compos. Struct. (2023), https://doi.org/10.1016/j.compstruct.2023.117329.
[4] Y. Pan, H. Li, Z. Du, Electrical/optical dual-energy-driven MXene fabric-based heater with fast response actuating and human strain sensing, J. Mater. Sci. Technol. (2024), https://doi.org/10.1016/j.jmst.2024.01.045.
[5] K. Keum, S.S. Cho, J.W. Jo, S.K. Park, Y.H. Kim, Mechanically robust textile-based strain and pressure multimodal sensors using metal nanowire/polymer conducting fibers, Iscience (2022), https://doi.org/10.1016/j.isci.2022.104032.
[6] S. Newby, M. Wajira, F. Anura, Modern developments for textile-based supercapacitors, ACS Omega 8 (14) (2023) 12613–12629. https://pubs.acs.org/doi/10.1021/acsomega.3c01176.
[7] S. Jo, J. Nagabandi, K. Daewon, Rational design of cobalt-iron bimetal layered hydroxide on conductive fabric as a flexible battery-type electrode for enhancing the performance of hybrid supercapacitor, J. Alloys Compd. (2022), https://doi.org/10.1016/j.jallcom.2022.164082.
[8] D. Wang, J. Sun, Q. Xue, Q. Li, Y. Guo, Y. Zhao, Z. Chen, Z. Huang, Q. Yang, G. Liang, B. Dong, C. Zhi, A universal method towards conductive textile for flexible batteries with superior softness, Energy Storage Mater. (2021), https://doi.org/10.1016/j.ensm.2021.01.001.
[9] L.R. Pahalagedara, I.W. Siriwardane, N.D. Tissera, R.N. Wijesenaa, K.M. Nalin de Silva, Carbon black functionalized stretchable conductive fabrics for wearable heating applications, RSC Adv. (2017), https://doi.org/10.1039/C7RA02184D.
[10] D. Wang, J. Dong, H. Ge, M. Tang, Q. Xie, J. Liu, Y. Si, Y. Wang, R. Sun, Electrically heated flexible heaters in wearable technology: a review of research progress and challenges, ACS Appl. Mater. Interfaces (2025), https://doi.org/10.1021/acsami.5c16961.

[11] J. Militký, K. Kupka, V. Tunáková, M. Venkataraman, Hybrid fabrics for ohmic heating applications, Polymers (2025), https://doi.org/10.3390/polym17101339.
[12] R. Manogaran, M. Malathi, A review on recent advancements in textile fabrics for electromagnetic interference (EMI) shielding materials, Mater. Today Commun. (2025), https://doi.org/10.1016/j.mtcomm.2025.111879.
[13] A.R. Sousa, S.A. Bunyaev, G.N. Kakazei, C. Freire, C.R. Pereira, A.M. Pereira, Architectural designs for efficient EMI-shielding textiles: from numerical simulations to screen-printing implementation, Mater. Des. (2025), https://doi.org/10.1016/j.matdes.2025.114371.
[14] E. Khajeh, K. Nasouri, G. Askari, M. Mandegari, Flexible and lightweight metalized polyamide nonwoven for electromagnetic interference shielding, electrothermal, photothermal, and antibacterial applications, Chem. Eng. J. (2024), https://doi.org/10.1016/j.cej.2024.158203.
[15] J. McCann, 12 - Collaborative design principles for smart clothing, in: J. McCann, D. Bryson (Eds.), Smart Clothes and Wearable Technology, Woodhead Publishing, 2023, pp. 283–325.
[16] M.R. Repon, A.D. Pranta, A. Haji, M.A. Jalil, Nanoparticles integrated antistatic textiles, in: M.R. Repon, D. Mikučioniene, A. Haji (Eds.), Nanoparticles Integrated Functional Textiles. Engineering Materials, Springer, Cham, 2025, pp. 177–203.
[17] M. Stoppa, A. Chiolerio, Wearable electronics and smart textiles: a critical review, Sensors (2014), https://doi.org/10.3390/s140711957.
[18] A. Asghar, M.R. Ahmad, M.F. Yahya, S.Z.U. Hassan, M. Kashif, Characterization based on the thermal capabilities of metallized fabrics equipped with hybrid conductive yarns for protective clothing, J. Text. Inst. (2018), https://doi.org/10.1080/00405000.2017.1423007.
[19] P. Du, J. Zhang, Z. Guo, H. Wang, Z. Luo, Z. Fan, B. Li, Z. Cai, F. Ge, A novel breathable flexible metallized fabric for wearable heating device with flame-retardant and antibacterial properties, J. Mater. Sci. Technol. (2022), https://doi.org/10.1016/j.jmst.2022.01.015.
[20] J. Chai, G. Wang, G. Wang, R. Shao, J. Zhao, G. Zhao, C.B. Park, Porous and conductive fiber woven textile for multi-functional protection, personal warmth, and intelligent motion/temperature perception, Adv. Funct. Mater. (2025), https://doi.org/10.1002/adfm.202416428.
[21] Y. Liu, M. Dai, R. Li, R. Hao, S. Wang, P. Hu, F. Sun, Z. Li, X. Hong, Humidity-triggered spontaneous phase separation enables multifunctional 3D porous composites for piezoresistive mechanosensory and electromagnetic interference shielding, Small (2026), https://doi.org/10.1002/smll.202509930.
[22] Y. Wei, R. Hao, X. Hong, S. Guo, D. Lu, H. Li, W. Zhao, Z. Tang, C. Zhou, W. Cao, X. Zheng, P. Hu, Z. Yu, S. Niu, Z. Han, L. Ren, W. Xu, S.C. Tan, Intelligent temperature and pressure sensing decoupling systems in multimodal nanonetwork-based electronic textiles, ACS Nano (2026), https://doi.org/10.1021/acsnano.6c03325.
[23] Z.M. Abay, Y. Wei, Z. Tang, Y. Liu, K. Chen, H. Li, Q. Wang, J. Yuan, P. Hu, D. Lu, C. Chen, X. Hong, Versatile MXene/(GO-AgNWs) electronic textile enabled by mixed-scale assembly strategy, NanoEnergy (2025), https://doi.org/10.1016/j.nanoen.2025.110963.
[24] A. Ojstršek, O. Plohl, S. Gorgieva, M. Kurečič, U. Jančič, S. Hribernik, D. Fakin, Metallisation of textiles and protection of conductive layers: an overview of application techniques, Sensors (2021), https://doi.org/10.3390/s21103508.
[25] J. Leśnikowski, Textile transmission lines in the modern textronic clothes, Fibres Text. East. Eur. 6 (89) (2011) 89–93.
[26] G.B. Tseghai, H.R. Tahir, B. Malengier, C. Hertleer, K.A. Fante, L. Van Langenhove, Smart textiles, in: R. Narayan (Ed.), Reference Module in Biomedical Sciences vol. 4, Elsevier, 2023, pp. 21–34.
[27] H. Qu, M. Skorobogatiy, 2 - Conductive polymer yarns for electronic textiles, in: T. Dias (Ed.), Electronic Textiles, Woodhead Publishing, 2015, pp. 21–53.
[28] B.E. Conway, R.E. White, Modern Aspects of Electrochemistry, Springer New York, 2002.
[29] H.H. Lou, Y. Huang, Electrplating, in: S. Lee (Ed.), Encyclopedia of Chemical Processing, Taylor and Francis, 2006, pp. 1–10.
[30] P. Xue, X. Tao, M.Y. Leung, H. Zhang, 5 – Electromechanical properties of conductive fibers, yarns and fabrics, in: X. Tao (Ed.), Wearable Electronics and Photonics, Elsevier, 2005, pp. 81–104.
[31] K.S. Sadanandan, A. Bacon, D.W. Shin, S.F.R. Alkhalifa, S. Russo, M.F. Craciun, A.I. S. Neves, Graphene coated fabrics by ultrasonic spray coating for wearable electronics and smart textiles, J. Phys. Mater. (2020), https://doi.org/10.1088/2515-7639/abc632.
[32] X. Zeyue, H. Ventura, M. Ardanuy, A review of the electrical conductivity test methods for conductive fabrics, Textiles (2024), https://doi.org/10.3390/textiles4030017.
[33] C.J.A. Cristancho, M.J.E. Rodriguez, G.C.A. Riviera, F. Roman, J.J. Pantoja, High current tests over conductive fabrics, in: 2018 International Conference on Electromagnetics in Advanced Applications (ICEAA), 2018, pp. 428–432.
[34] C.J.A. Cristancho, M.J.E. Rodriguez, G.C.A. Riviera, F. Roman, A. Piantini, M. Shigihara, C.Y. Kodaira, Behavior of an electroconductive rip-stop fabric under 8/20 μs lightning current: preliminary results, in: 2021 35th International Conference on Lightning Protection (ICLP) and XVI International Symposium on Lightning Protection (SIPDA), 2021, pp. 01–04.
[35] F. Román, D. Rodriguez, M. Rahman, A. Lobato, J. Rodriguez, J. Cristancho, C. Acosta, 10/350 μs lightning impulse current behavior of a conductive fabric, in: 2021 35th International Conference on Lightning Protection (ICLP) and XVI International Symposium on Lightning Protection (SIPDA), 2021, pp. 01–06.
[36] IEC 61000-4-5, in: Electromagnetic Compatibility (EMC). Testing and Measurement Techniques. Surge Immunity Test, International Electrotechnical Commission, 1995.
[37] Z. Tang, W. Sun, C. Tao, T. Peng, H. Li, K. Chen, J. Li, Z. Zhao, Z. Li, X. Hong, Rapid response, superior stable, and durable pressure sensor with rGO/CNC interdigital electrode, NanoEnergy (2024), https://doi.org/10.1016/j.nanoen.2024.110041.